PNAS RESEARCH ARTICLE | CELL BIOLOGY

Piezo mechanosensory channels regulate centrosome integrity and mitotic entry

Liron David[a,b,1], Laurel Martinez[c,d], Qiongchao Xi[c], Kameron A. Kooshesh[c,3,4], Ying Zhang[c,2], Jagesh V. Shah[e,f], Richard L. Maas[c,1], and Hao Wu[a,b,1]

Contributed by Hao Wu; received August 11, 2022; accepted November 23, 2022; reviewed by Iain Cheeseman and Miguel A. Valverde

Piezo1 and 2 are evolutionarily conserved mechanosensory cation channels known to function on the cell surface by responding to external pressure and transducing a mechanically activated Ca^{2+} current. Here we show that both Piezo1 and 2 also exhibit concentrated intracellular localization at centrosomes. Both Piezo1 and 2 loss-of-function and Piezo1 activation by the small molecule Yoda1 result in supernumerary centrosomes, premature centriole disengagement, multi-polar spindles, and mitotic delay. By using a GFP, Calmodulin and M13 Protein fusion (GCaMP) Ca^{2+}-sensitive reporter, we show that perturbations in Piezo modulate Ca^{2+} flux at centrosomes. Moreover, the inhibition of Polo-like-kinase 1 eliminates Yoda1-induced centriole disengagement. Because previous studies have implicated force generation by microtubules as essential for maintaining centrosomal integrity, we propose that mechanotransduction by Piezo maintains pericentrosomal Ca^{2+} within a defined range, possibly through sensing cell intrinsic forces from microtubules.

piezo | mechanotransduction | centrosomes | Ca^{2+} signaling | centrioles

Piezo1 and Piezo2 are mechanosensory cation channels discovered as the primary responders to cell membrane pressure in vertebrates with homologs in other organisms (1). Because of their Ca^{2+}-permeability, Piezo1 and Piezo2 can transduce a mechanically activated Ca^{2+} current into cells (2–4) and thus perform a wide range of biological functions from vascular development, blood pressure control, and red cell volume control (5–11), to touch sensation and proprioception (10–13). Both *PIEZO1* and *PIEZO2* gain- and loss-of-function mutations are associated with severe human diseases (14). In particular, we and others have shown that *PIEZO2* gain-of-function mutations cause pleiotropic musculoskeletal contracture syndromes, including distal arthrogryposis type 5, Gordon syndrome, and Marden-Walker syndrome, while *PIEZO2* loss-of-function causes distal arthrogryposis with impaired proprioception and touch (15–19). In an effort to investigate the function of Piezo2 in muscle development, we discovered a general function of Piezo1 and 2 intracellularly in controlling centrosome integrity, suggesting that Piezo proteins may represent an important new class of intracellular mechanotransducers.

Results

Piezo1 and 2 Localize at Centrosomes. To address the role of Piezo proteins in muscle development, we used the undifferentiated C2C12 myoblast cell line for immunofluorescence (IF). Using different antibodies and different fixation methods, we found that Piezo2 exhibited punctate intracellular distribution with strong foci co-stained with the centrosomal marker γ-tubulin, in either interphase or mitotic C2C12 cells (Fig. 1*A* and *SI Appendix*, Fig. S1 *A–C*). This centrosomal localization of Piezo2 was further validated in the IMCD3 kidney epithelial cell line (20) and the Neuro-2A mouse neuroblastoma cell line (Fig. 1*B* and *SI Appendix,* Fig. S1*D*). Piezo1 also displayed centrosomal localization in the different cell lines, in either interphase or mitosis (Fig. 1 *C* and *D* and *SI Appendix,* Fig. S1 *E* and *F*), although this localization is among the background of a more complex intracellular distribution in comparison with Piezo2. Live imaging of Green Fluorescent protein (GFP) fluorescence in C2C12 cell line stably expressing Piezo1-GFP revealed dynamic Piezo1 localization during the cell cycle and confirmed its especially strong localization at the mitotic spindle (*SI Appendix* Fig. S1 *G–I* and Movie S1). To verify the centrosomal localization in vivo, we examined by IF of tissue sections of wild-type (WT) mice and *Piezo2*$^{-/-}$ mice that are less embryonically lethal than *Piezo1*$^{-/-}$ mice (8, 21). We observed Piezo protein puncta that overlapped with γ-tubulin-marked centrosomes in WT mice (*SI Appendix* Fig. S2*A*), and lack of such staining in *Piezo2*$^{-/-}$ littermate (*SI Appendix* Fig. S2 *B–H*). Cell surface, nuclear envelope, and endoplasmic reticulum localizations have all been reported for Piezo proteins (22–24). In addition, Piezo1 was recently shown to localize

Significance

Piezo1 and 2 are mechanosensory channels known to be responsible for sensing mechanical stimuli on the cell membrane. They are widely expressed, play important roles in developmental and homoeostatic processes and are involved in human diseases such as anemia, musculoskeletal disorders and cancer. Piezo proteins are involved in migration, invasion, and proliferation of cancer cells, due to upregulation or downregulation of Piezo in different cancer types. Our study proposes a new intracellular role for Piezo proteins in cell cycle progression by regulating centrosome integrity. We show that either up- or downregulation of Piezo channels results in supernumerary centrosomes, a hallmark of cancer. Thus, Piezo proteins may serve as potential biomarkers and important targets for therapeutic intervention in cancer.

Reviewers: I.C., Whitehead Institute for Biomedical Research; and M.A.V., Universitat Pompeu Fabra.

The authors declare no competing interest.

[1]To whom correspondence may be addressed. Email: david@crystal.harvard.edu, rmaas@bwh.harvard.edu, or wu@crystal.harvard.edu.

[2]Present address: Medical Research Institute, Wuhan University, Hubei 430071, China.

[3]Present address: Department of Medicine and Center for Regenerative Medicine, Massachusetts General Hospital, Boston, MA 02114

[4]Present address: Department of Stem Cell and Regenerative Biology and Harvard Stem Cell Institute, Harvard University, Cambridge, MA, 02138

This article contains supporting information online at https://www.pnas.org/lookup/suppl/doi:10.1073/pnas.2213846120/-/DCSupplemental.

Published December 27, 2022.

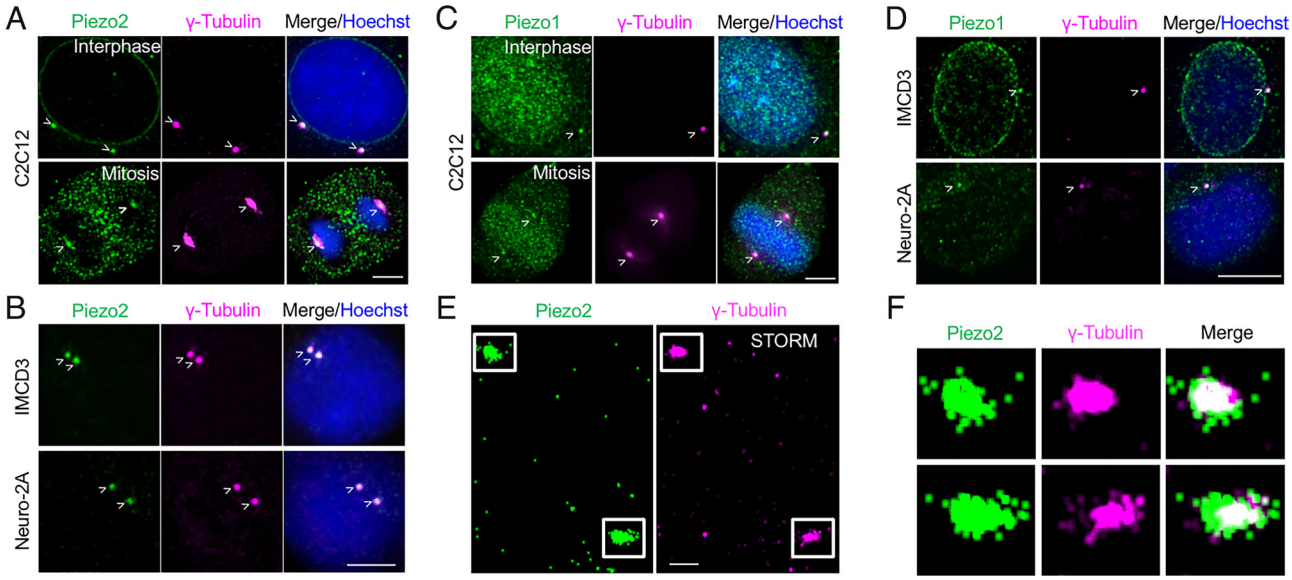

Fig. 1. Piezo1/2 localization to centrosomes. (*A* and *B*) Centrosome localization of Piezo2 in C2C12 myoblast cells (*A*) and in IMCD3 and Neuro-2A cells (*B*) visualized by IF for Piezo2 (green), γ-Tubulin (magenta), and DNA (Hoechst dye, blue) in mitotic and interphase cells. (*C* and *D*) Centrosome localization of Piezo1 in C2C12 myoblast cells (*C*) and in IMCD3 and Neuro-2A cells (*D*) visualized by IF for Piezo1 (green), γ-Tubulin (magenta), and DNA (Hoechst dye, blue) in mitotic and interphase cells. (*E* and *F*) Two-color STORM of Piezo2 (green) and γ-Tubulin (magenta) (*E*) and 3× enlarged *Insets* (*F*). The data suggest that Piezo2 is localized at the pericentrosomal region with a distribution wider than that of γ-Tubulin.

to the intercellular bridge during cytokinesis (25), a finding that we also observed (*SI Appendix*, Fig. S1*G* and Movie S1). However, centrosomal localization has not been recognized previously.

To more precisely localize Piezo proteins at the centrosome, we performed super-resolution imaging on C2C12 cells co-stained with Piezo2 and γ-tubulin, using stochastic optical reconstruction microscopy (STORM) (Fig. 1 *E* and *F*) and instant structured illumination microscopy (iSIM) (*SI Appendix*, Fig. S3). Piezo2 co-localized with γ-tubulin, but was more disperse than γ-tubulin and even appeared vesicular at the periphery of the foci (Fig. 1*F*).

Piezo1 or 2 Knockout or Knockdown Induced Supernumerary Centrosomes and Mitotic Delay. To investigate the potential function of Piezo proteins on centrosomes, we performed CRISPR-Cas9 polyclonal knockout (pKO) of Piezo1 or Piezo2 in C2C12 cells (*SI Appendix*, Fig. S4*A*), because the selection of KO clones was not possible due to cell death. Strikingly, we detected by IF imaging many cells with three or more centrosomes, a phenotype known as supernumerary centrosomes (26, 27), as well as with misaligned spindles (Fig. 2*A* and *SI Appendix*, Fig. S4 *B* and *C*). The quantification of IF images revealed that 35 to 53% of Piezo pKO C2C12 cells in interphase or mitosis exhibited supernumerary centrosomes, in comparison with 12% for off-target Rosa26 pKO (Fig. 2*B*). Supernumerary centrosomes were also observed in 22 to 45% of C2C12 cells following short hairpin RNA (shRNA) knockdown (KD) of Piezo1 or 2 compared to 4 to 10% in control cells receiving a control shRNA (*SI Appendix*, Fig. S4 *D*–*F*). Thus, Piezo1 and 2 are not only localized at centrosomes, but are also required for regulation of centrosome number.

To determine whether Piezo pKO in C2C12 cells caused mitotic defects, we synchronized these cells at the G2/M border by a 12-h treatment with the cyclin-dependent kinase 1 inhibitor RO-3306 (RO) (28). We then washed out the inhibitor to release the cell cycle arrest and fixed the cells 45 min after. When visualized by IF for both α-tubulin and γ-tubulin, C2C12 cells transduced with off-target Rosa26 pKO showed predominantly normal dividing cells with bipolar spindles (Fig. 2*C*). Piezo1 and 2 pKO cells at early stages of mitosis (e.g., prometaphase) showed supernumerary centrosomes and misaligned or multipolar spindles (Fig. 2*C*). The quantitative analysis revealed significant accumulation of Piezo1 and 2 pKO cells in prometaphase compared to off-target cells and less cells in late mitosis (Fig. 2*D*). Strikingly, when we performed pKO for both Piezo1 and 2 (double pKO) in C2C12 cells (*SI Appendix*, Fig. S4*A*), only 2% of the cells were mitotic cells with severe mitotic entry arrest at 30 min after RO release of G2/M synchronization, in comparison with 24% mitotic cells for WT C2C12, 7% for Piezo1 pKO and 13% for Piezo2 pKO (Fig. 2 *E* and *F*). Thus, Piezo proteins may redundantly play a considerable role in regulating mitotic entry.

We next sought to determine whether the supernumerary centrosome phenotype associated with Piezo pKO in C2C12 cells also occurred in vivo. Primary myoblasts from WT and *Piezo2*$^{-/-}$ littermate newborn mice (11) were isolated from skeletal muscles and passaged to enrich for myoblasts (29). Co-Immunofluorescence (Co-IF) revealed Piezo2 staining at γ-tubulin-marked centrosomes and normal numbers of centrosomes in 75 to 80% of WT primary myoblasts (Fig. 2 *G* and *H*). By contrast, *Piezo2*$^{-/-}$ myoblasts displayed supernumerary centrosomes in 45 to 55% of myoblasts (Fig. 2 *G* and *H*), resembling those in CRISPR-Cas9 pKO or shRNA KD cells. In addition, cell cycle analysis by flow cytometry revealed a significant accumulation of *Piezo2*$^{-/-}$ cells (56%) in G2/M in comparison with WT cells (25%), with a corresponding decrease in cells in G0/G1 (Fig. 2*I*). This G2/M accumulation phenotype for *Piezo2*$^{-/-}$ cells is similar to that shown for Piezo pKO in C2C12 cells.

Pharmacologic Activation and Inhibition of Piezo Protein-Induced Supernumerary Centrosomes. We employed known pharmacological modulators of Piezo proteins to assess the immediate effects of Piezo activity alteration on centrosomes. Yoda1, a cell-permeable small molecule activator of Piezo1 that induces channel opening in the absence of mechanical force (30, 31), was used at 10 μM, the midpoint of the previously established dose–response curve. C2C12 cells synchronized to the G2/M border were given Yoda1, and analyzed at 30 min by IF for α-tubulin and γ-tubulin. Approximately 50% of the mitotic cells exhibited supernumerary centrosomes with misaligned or

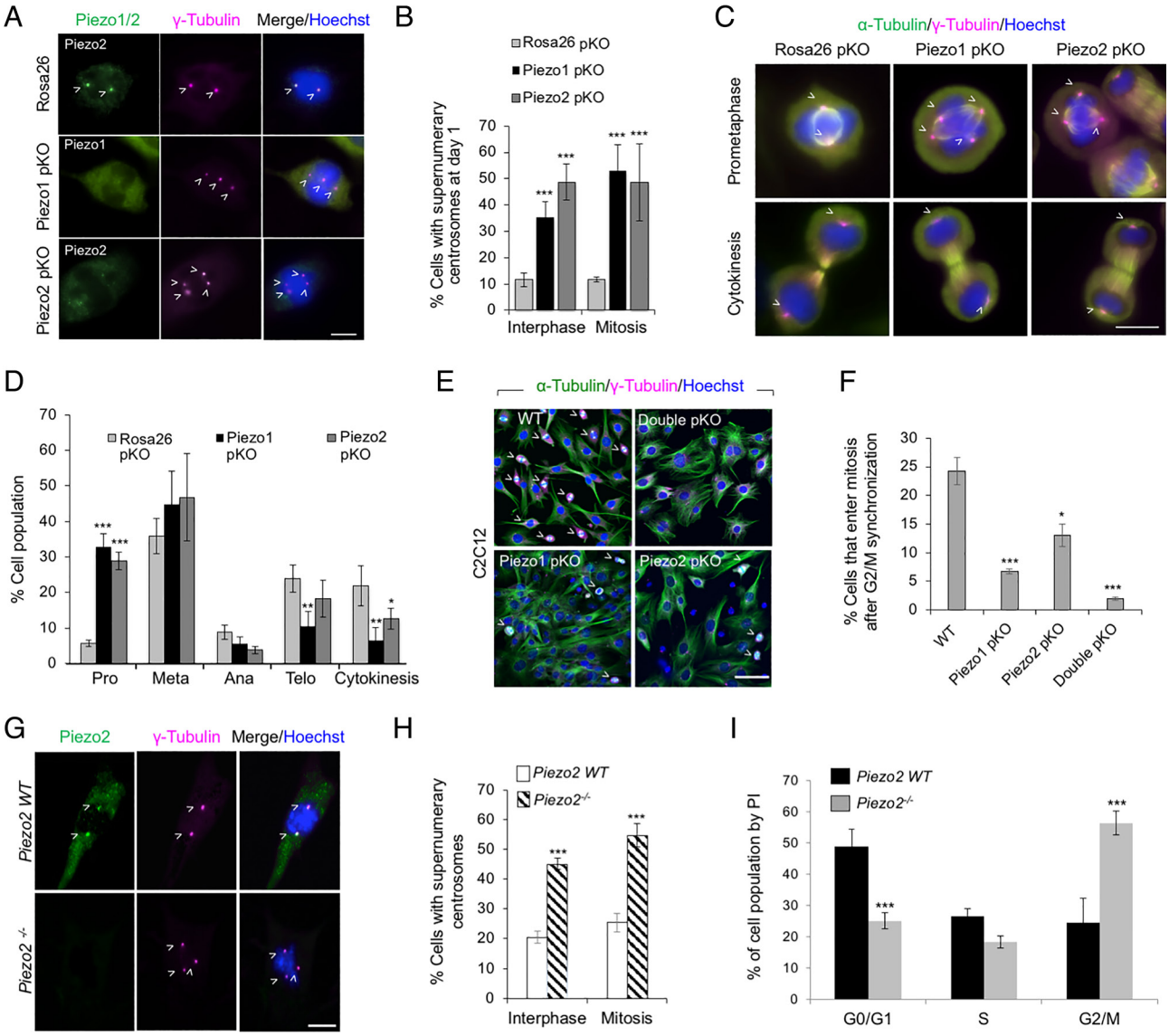

Fig. 2. Supernumerary centrosomes associated with Piezo1/2 pKO or *Piezo2*$^{-/-}$. (*A*) CRISPR-Cas9 pKO for Rosa26 (off target control), Piezo1 or Piezo2 in C2C12 cells at day 1 post selection imaged by IF as in Fig. 1 *A*–*C*, showing supernumerary centrosomes in mitotic cells. (*B*) Quantitative analysis of supernumerary centrosomes in interphase and mitotic C2C12 pKO cells from the IF experiments in (*A*) and *SI Appendix*, Fig. S4*B*. (*C*) Rosa26, Piezo1 or Piezo2 pKO C2C12 cells at day 1 post selection and 45 min after release of G2/M border synchronization with RO-3066, imaged by IF for α-Tubulin (green), γ-Tubulin (magenta) and DNA (Hoechst dye, blue). (*D*) Quantitative analysis of mitotic cell populations from the IF experiments in (*C*). In three independent experiments, 190 to 280 cells were scored for each category based on the mitotic stage. Pro: prometaphase, Meta: metaphase, Ana: anaphase, Telo: telophase, Cyto: cytokinesis, scored as per Methods. (*E*) Representative field views of Piezo1 pKO, Piezo2 and double pKO cells visualized by IF 30 min after RO-3306 release in comparison with WT C2C12 cells, showing paucity of mitotic cells by double pKO. Cells were imaged by IF for α-Tubulin (green), γ-Tubulin (magenta) and DNA (Hoechst dye, blue). Mitotic cells are labeled with white arrowheads. (*F*) Quantitative analysis for the number of cells that entered mitosis from IF experiments in (*E*). (*G*) *Piezo2*$^{-/-}$ myoblasts derived from newborn mice imaged by IF as in (*A*), showing supernumerary centrosomes in *Piezo2*$^{-/-}$ myoblasts. (*H*) Quantitative analysis of supernumerary centrosomes in interphase and mitotic cells in WT and *Piezo2*$^{-/-}$ myoblasts from IF experiments in (*G*). (*I*) Cell cycle analysis by flow cytometry for WT and *Piezo2*$^{-/-}$ myoblasts. All images are maximum intensity Z projections. Centrosomes and centrosome-localized Piezo proteins are marked with white arrowheads (*A*, *C*, and *G*). (Scale bars are 5 μm (*E*) and 10 μm (*A*, *C*, and *G*).) For (*F* and *H*), data are represented by mean ± SEM from three independently quantified experiments counting 50 to 200 cells each. Statistical significance between an experimental group and a control group was assessed by one-way ANOVA or two-tailed *t* test with ***, ** and * denote $P < 0.0001$, 0.001 and 0.01, respectively.

multipolar spindle organization, in comparison with 12% for those that received the Dimethylsulfoxide (DMSO) vehicle (Fig. 3 *A* and *B*). Moreover, similar to Piezo1 pKO cells, Piezo1 activation by Yoda1 or calcium depletion by the BAPTA-AM Ca^{2+} chelator led to mitotic entry delay, resulting in 50% reduction in the number of cells that entered mitosis, in comparison with DMSO control (Fig. 3 *C* and *D*). Hence, these data further support that Piezo proteins have a role in regulating mitotic entry.

Co-treatment with 10 μM Yoda1 and 10 μM Dooku1, a modified Yoda1 analog that is mildly agonistic alone but antagonizes Yoda1 when used together (32), reduced the percentage of cells with supernumerary centrosomes to 40% (Fig. 3*B*). With Dooku1 alone, the number of cells with supernumerary centrosomes was 25% (Fig. 3*B*). Yoda1-treated cells, but not untreated cells, exhibited thin, extended F-actin positive (marked by phalloidin) cell surface protrusions (Fig. 3*E* and *SI Appendix*, Fig. S5*A*), a phenotype that has been previously observed with Yoda1 treatment (33).

To investigate whether the effects of Yoda1 and Dooku1 were due to cell surface or intracellular Piezo1 activation, we used Piezo1 activators Jedi1 and Jedi2, which activate Piezo1 only from

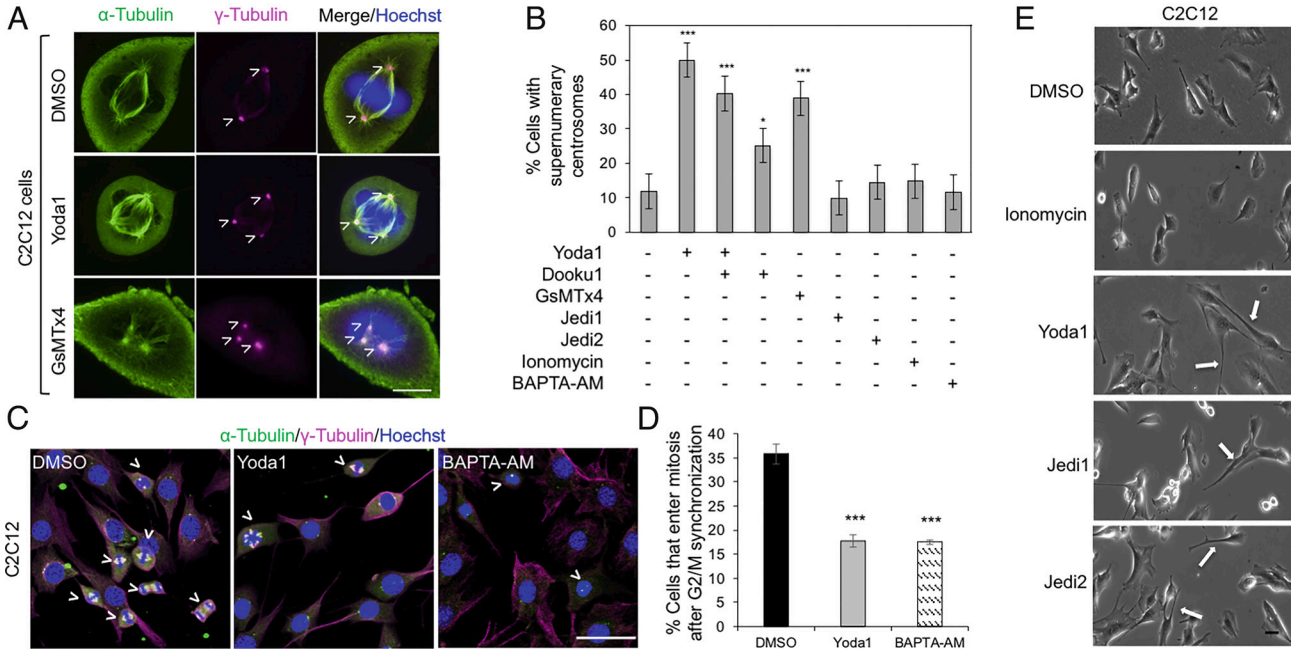

Fig. 3. Supernumerary centrosomes and mitotic entry delay upon Piezo pharmacological activation or inhibition. (*A*) C2C12 cells treated for 30 min with DMSO (0.1%, vehicle control), Yoda1 (Piezo1 activator, 10 μM) or GsMTx4 (mechanosensitive channel inhibitor, 5 μM) after RO-3066 release. Cells were imaged by IF for α-Tubulin (green), γ-Tubulin (magenta) and DNA (Hoechst dye, blue). (*B*) Quantitative analysis for percentage of C2C12 cells with supernumerary centrosomes from IF images similar to (*A*) following treatment with DMSO (0.1%), Yoda1 (10 μM), Yoda1 plus Dooku1 (10 μM each), Dooku1 (10 μM), GsMTx4 (5 μM), Jedi1 (200 μM), Jedi2 (200 μM), ionomycin (10 μM) or BAPTA-AM (40 μM). (*C*) Representative field views of C2C12 cells treated with DMSO, Yoda1 or BAPTA-AM after RO-3306 release for 30 min and visualized by IF for α-Tubulin (green), γ-Tubulin (magenta) and DNA (Hoechst dye, blue). Mitotic cells are labeled with white arrowheads. (*D*) Quantitative analysis for the number of cells that entered mitosis from IF experiments in (*C*). (*E*) Phase images of C2C12 cells 30 min after treatment with DMSO, ionomycin, Yoda1, Jedi1 and Jedi2 under the same condition as in (*B*). Yoda1, Jedi1 or Jedi2 treatment, but not DMSO or ionomycin treatment, led to cell surface protrusions due to plasma membrane Piezo1 activation. (All scale bars are 10 μm, except in (*C*) which is 4 μm.) For (*D*), data are represented by mean ± SEM from three independently quantified experiments counting 50 to 200 cells each. Statistical significance for Fig. 3*B* was assessed by one-way ANOVA test and for Fig. 3*D*, statistical significance between an experimental group and a control group was assessed by two-tailed *t* test with ***, ** and * denote $P < 0.0001$, 0.001 and 0.01, respectively.

the extracellular side and are not cell permeable shown by patching clamping (34). The treatment of C2C12 cells with either Jedi1 or Jedi2 at 200 μM, a concentration at or above the mid-point of the dose–response curve (34), did not cause an increase in supernumerary centrosomes (Fig. 3*B* and *SI Appendix,* Fig. S5*B*), but resulted in cell surface protrusions (*SI Appendix,* Fig. S5 *B* and *C*), supporting that Jedi1 and Jedi2 exerted their expected effect. In addition, we used ionomycin, a Ca^{2+} ionophore that induces intracellular Ca^{2+} influx and found that ionomycin did not induce supernumerary centrosomes and did not lead to cell surface protrusions (Fig. 3 *B–D* and *SI Appendix*, Fig. S5*B*). These data suggest that aberrant activation of intracellular Piezo1, but not of cell surface Piezo1 or general Ca^{2+} influx, deregulates normal centrosomal number.

To further determine whether the induction of supernumerary centrosomes by Yoda1 could be attributed to off-target effects, Piezo1 pKO C2C12 cells were treated with either Yoda1 or DMSO. Because of the lack of Piezo1 in these cells, Yoda1 treatment should have no effects, and indeed, a similar percentage of these cells exhibited supernumerary centrosomes with or without Yoda1 treatment (*SI Appendix*, Fig. S5*D*). By contrast, Rosa26 pKO C2C12 cells showed increased percentage of cells with supernumerary centrosomes in the presence of Yoda1 in comparison with DMSO control, similar to WT C2C12 cells (*SI Appendix*, Fig. S5*D*). These data are reassuring of the striking phenotypes we observed.

We used GsMTx4 peptide, a spider venom toxin that inhibits Piezo1 and 2 as well as other mechanosensitive cation channels (35–38) to investigate the consequence of Piezo pharmacologic inhibition. Interestingly, similar to Yoda1 treatment, GsMTx4 treatment also significantly increased the number of cells with supernumerary centrosomes to 39% (Fig. 3 *A* and *B* and *SI Appendix*, Fig. S5*B*). As with lack of centrosomal phenotype when treated with ionomycin, treatment with BAPTA-AM, a cell-permeable Ca^{2+} chelator, also did not lead to supernumerary centrosomes in comparison with untreated cells (Fig. 3*B*). Thus, both pharmacologic activation of Piezo1 and inhibition of mechanosensitive ion channels including Piezo1 and 2 produced supernumerary centrosomes. While the supernumerary centrosome phenotype with Yoda1 was surprising, the appearance of a similar phenotype with GsMTx4 treatment, presumably reflecting Piezo inhibition, is consistent with the results in Piezo pKO and KD C2C12 cells and in *Piezo2*$^{-/-}$ myoblasts.

Piezo Activation and Inhibition-Induced Premature Centriole Disengagement. To determine whether the supernumerary centrosomes that form upon Piezo activation or inhibition result from centrosome over-duplication, premature centriole disengagement, centrosome fragmentation or some other mechanism (39–41), we generated a C2C12 cell line that stably expressed GFP-Centrin2. Unlike γ-tubulin, a component of the pericentriolar material that does not distinguish each centriole, Centrin2 is a component of the centriole per se, and can individually mark mother and daughter centrioles. We added 10 μM Yoda1 to GFP-Centrin2 C2C12 cells, either unsynchronized (Fig. 4*A*) or synchronized at G2/M by RO (Fig. 4*B*), and analyzed the cells for GFP and by anti-γ-tubulin IF. Strikingly, upon Piezo1 activation by Yoda1, premature centriole disengagement of one or

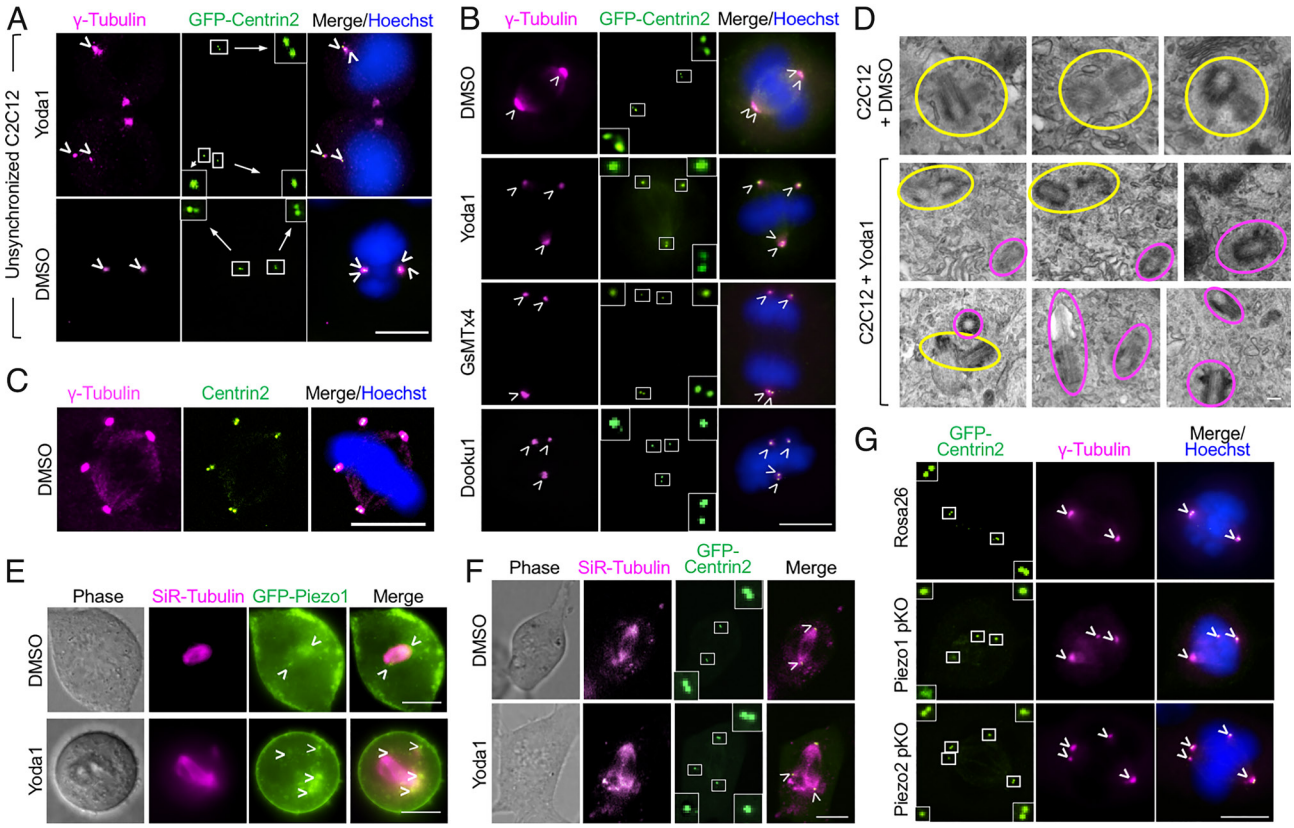

Fig. 4. Premature centriole disengagement upon Piezo pharmacological activation or inhibition. (*A*) Unsynchronized C2C12 cells expressing GFP-Centrin2 (green), fixed 30 min after introducing Yoda1 (10 μM) or DMSO (0.1%, vehicle control) and stained for γ-Tubulin (magenta) and DNA (Hoechst, blue). Yoda1 treatment resulted in centriole disengagement. (*B*) C2C12 cells stably expressing GFP-Centrin2 treated for 30 min with DMSO, Yoda1, GsMTx4 or Dooku1 after RO-3066 release, showing supernumerary centrosomes and centriole disengagement. Cells were imaged by IF for γ-Tubulin (magenta), Centrin2 (GFP fluorescence) and DNA (Hoechst dye, blue). Rectangular boxes encircle centrosomes, and their zoom-in views are displayed. (*C*) Supernumerary centrosomes in RO-3306-synchronized C2C12 cells expressing GFP-Centrin2 (green) fixed 30 min after introducing 0.1% DMSO and stained for γ-Tubulin (magenta) and DNA (Hoechst, blue). The low percentage of supernumerary centrosomes in DMSO control was resulted from centriole duplication, not centriole disengagement. (*D*) EM gallery of centrosomes, imaged in thin plastic sections of embedded C2C12 cells 1 h after treatment with of DMSO (*Top*) or Yoda1 (*Bottom*). Yellow and magenta circles mark pairs of mother and daughter centrioles, and separated centrioles, respectively. (*E* and *F*) Live fluorescent and phase images of mitotic C2C12 cells stably expressing GFP-Piezo1 (green) (*E*) or GFP-Centrin2 (*F*). Cells were treated with DMSO or Yoda1 together with SiR-Tubulin for staining microtubules (magenta) after release of RO-3306-mediated cell cycle synchronization and imaged 30 min later. Misaligned spindles following Yoda1 treatment are apparent from SiR-Tubulin staining. Rectangular boxes in (*F*) encircle centrosomes, and their zoom-in views are displayed. (*G*) Piezo1 and 2 pKO C2C12 cells stably expressing GFP-Centrin2 at day 1 post-KO selection and RO-3306 synchronization. Cells were washed out and visualized by IF for Centrin2 (GFP fluorescence), γ-Tubulin (magenta) and DNA (Hoechst, blue). All images are maximum intensity Z projections. (All scale bars are 10 μm except in (*D*) which is 200 nm.)

two centrosomes occurred, resulting in the formation of individual centrioles. Separated centrioles were also identified following either GsMTx4 or Dooku1 treatment (Fig. 4*B*). For DMSO control after RO treatment, we did not observe separated centrioles. The low percentage of cells with supernumerary centrosomes in these cells resulted from centriole duplication (Fig. 4*C*), which further validates that the centriole disengagement phenotype observed is due to perturbations in Piezo and not an artifact due to RO treatment.

The average distance measured between the two disengaged centrioles 30 min post Yoda1 treatment was 4.97 ± 0.85 μm, compared to 0.56 ± 0.03 μm before treatment and 0.54 ± 0.02 μm 30 min post-DMSO treatment (*SI Appendix*, Fig. S6*A*). The same centriole disengagement was observed upon Yoda1 treatment when Pericentrin, another component of the pericentriolar material as γ-tubulin, was used in co-IF to mark the centrosome location (*SI Appendix*, Fig. S6*B*). For distinguishing mother and daughter centrioles, we used Cep164, a mother centriole marker. By imaging mitotic C2C12 cells treated with Yoda1 and performing co-IF for Cep164 and γ-tubulin, we observed that upon premature centriole disengagement, the daughter centriole preferentially moved away from its original position at one end of the mitotic spindles, while the mother centriole appeared to remain stationary at the end of the mitotic spindle (*SI Appendix*, Fig. S6*C*). In order to further demonstrate the phenotype observed, we also used transmission electron microscopy (TEM) to confirm the distance of disengagement between free centrioles, which was frequently >3.5 μm, compared to ~200 nm in WT C2C12 cells (Fig. 4*D* and *SI Appendix*, Fig. S6*D*).

In order to visualize the effect on mitotic spindle upon treatment with Yoda1, we imaged Piezo1-GFP C2C12 and GFP-Centrin2 C2C12 cells with the live cell dye SiR-Tubulin to stain microtubules. We identified misaligned spindles following 10 μM Yoda1 stimulation (Fig. 4 *E* and *F*). To extend these findings to other cells, we tested the IMCD3 cell line, which also exhibited Piezo1 and 2 co-localization with centrosomes (Fig. 1 *B*–*D*). Similar to C2C12 cells, treatment with Yoda1 or GsMTx4 resulted in 40% or 42% of IMCD3 cells, respectively, having supernumerary centrosomes and multipolar spindles 30 min after treatment (*SI Appendix*, Fig. S6 *E* and *F*).

Piezo KO Induced Premature Centriole Disengagement. Centriole disengagement as a potential mechanism for supernumerary centrosomes in both Yoda1- and GsMTx4-treated C2C12 cells

prompted us to consider whether a similar mechanism could account for the supernumerary centrosomes in Piezo1 and 2 pKO cells. We performed CRISPR-Cas9 pKO of Piezo1 and 2 in C2C12 cells stably expressing GFP-centrin2, and imaged the locations of GFP-Centrin2 and γ-tubulin. The supernumerary centrosomes in these cells contained either two centrioles, or a single centriole (Fig. 4*G* and *SI Appendix*, Fig. S6*G*), as observed for cells with pharmacologically activated or inhibited Piezo proteins. Thus, centrosome disengagement to form single centrioles occurs in Piezo pKO cells. However, likely due to the longer duration of the KO protocol, centriole replication to form intact centrosomes also occurred (27).

To test this idea further, we imaged GFP-Centrin2 C2C12 cells after either a 30-min or an extended 24-h incubation with Yoda1, or after a 30-min treatment with Yoda1 followed by a 24-h recovery. Each treatment yielded progressively lower percentages of cells with isolated centrioles and increasing numbers with supernumerary centrosomes containing paired centrioles (*SI Appendix*, Fig. S6 *H* and *I*). These results are also consistent with the idea that free centrioles form in Piezo pKO cells, with some replicating to form intact centrosomes over time. Thus, both Piezo loss- and gain-of-function states appear to produce similar premature centriole disengagement phenotypes, suggesting that a critical range of Piezo activity is required to maintain centrosome integrity likely by mechanotransduction of microtubule forces.

Rapid Premature Centriole Disengagement upon Piezo1 Activation in Early and Late Mitotic Stages but not Metaphase. To gain further insight into the kinetics of the centriole dissociation process, we synchronized GFP-Centrin2 C2C12 cells that also expressed H2B-mCherry to mark chromatin at G2/M with RO. At 15 min, 30 min, or 45 min after RO washout, we added Yoda1 or DMSO vehicle, and imaged these cells at early, middle or late stage of mitosis, respectively (Fig. 5 *A*–*C* and *SI Appendix*, Fig. S7*A* and Movies S2–S5). With DMSO vehicle, intact centrosomes migrated to the spindle poles and the centrioles maintained tight coupling throughout the imaging period (*SI Appendix*, Fig. S7*A* and Movie S2). With Yoda1 treatment, we observed rapid centriole disengagement within a few minutes for cells at early mitotic stage (prophase), resulting in misaligned spindles and lagging chromatin marked by H2B-mCherry (Fig. 5*A* and Movie S3). Rapid centriole disengagement was also observed for cells at late mitotic stage (cytokinesis) (Fig. 5*C* and Movie S5).

However, no centriole disengagement was observed for cells at middle mitotic stage (metaphase) (Fig. 5*B* and Movie S4). We further synchronized cells to metaphase by treatment with

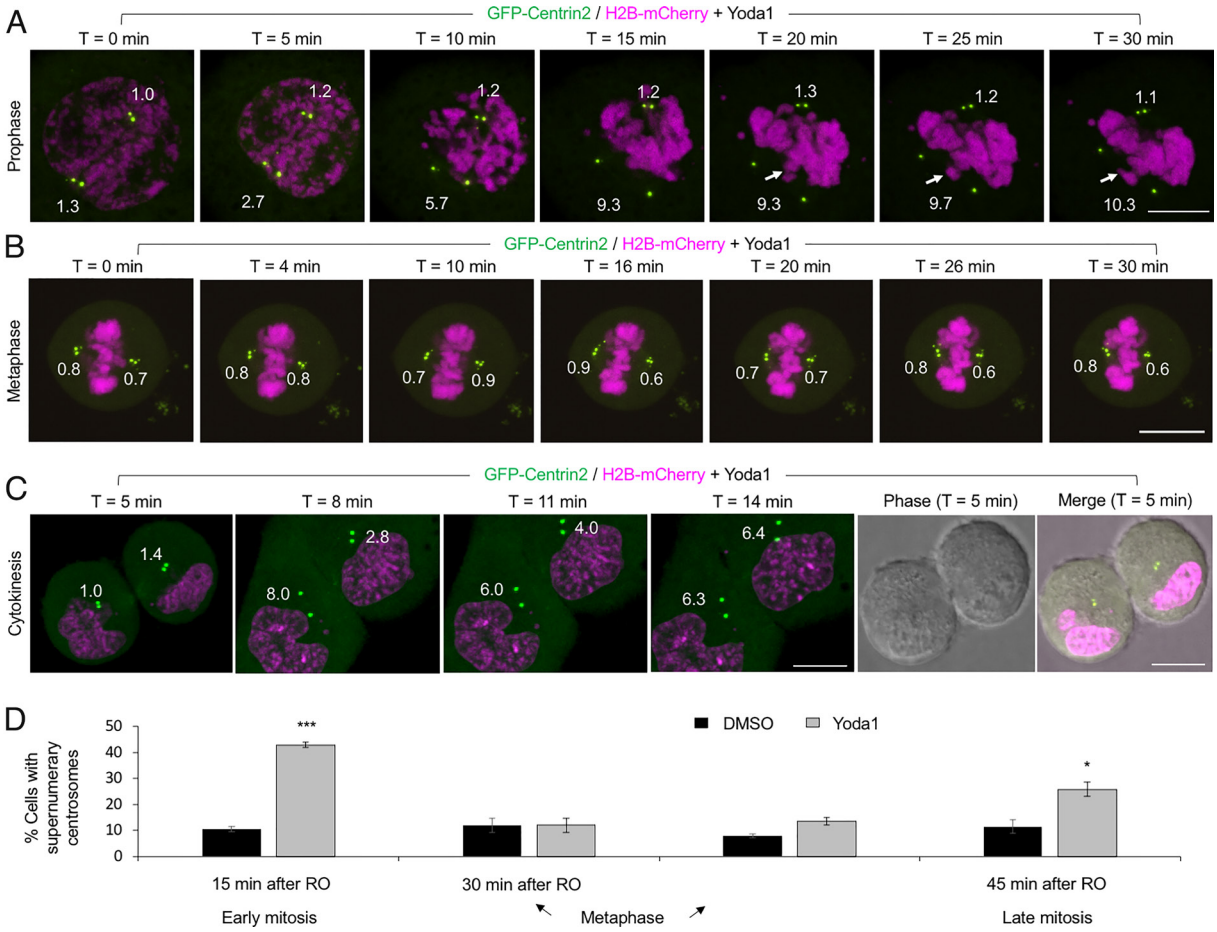

Fig. 5. Rapid centriole disengagement following Yoda1 treatment during mitosis. (*A*–*C*) Live time-lapse images from mitotic C2C12 cells stably expressing GFP-Centrin2 (green) and H2B-mCherry (magenta) treated with Yoda1 (10 μM). Cells were synchronized to G2/M by RO-3306 and Yoda1 was introduced 15 min (*A*), 30 min (*B*) and 45 min (*C*) after RO-3306 washout to capture cells at prophase (*A*), metaphase (*B*) and cytokinesis (*C*), respectively. Phase images are shown for (*C*) to emphasis the mitotic stage. Distances (μm) between mother and daughter centriole pairs are marked, and lagging chromatin in (*A*) is labeled by white arrows. Rapid centriole disengagement was observed at prophase and cytokinesis; however, cells at metaphase did not exhibit centriole disengagement upon Yoda1 introduction. (*D*) Quantitative analysis of IF images of C2C12 cells for supernumerary centrosomes following treatment with DMSO (0.1%) or Yoda1 (10 μM) at different mitotic stages, captured as in *SI Appendix*, Fig. S7*C*. All images are maximum intensity Z projections. (All scale bars are 10 μm.) Data in (*D*) are represented by mean ± SEM from three independently quantified experiments counting 100 to 250 cells each. Statistical significance between an experimental group and a control group was assessed by two-tailed *t* test with *** and * for $P < 0.0001$ and 0.01, respectively.

MG132, a proteasome inhibitor (42), and confirmed lack of centriole disengagement at metaphase (*SI Appendix*, Fig. S7*B* and Movie S6). We speculate that at metaphase when the chromosomes are already aligned at the spindles, the forces are so strong that Piezo activation will not have an effect at that specific checkpoint.

To obtain quantitative data on centriole disengagement and the cell cycle, we also imaged fixed C2C12 cells that were synchronized and treated with Yoda1, and counted cells with supernumerary centrosomes (Fig. 4*D* and *SI Appendix*, Fig. S7*C*). We detected that the most significant population of cells with supernumerary centrosomes comprises early mitotic cells with 43% of cells at prophase and prometaphase exhibiting supernumerary centrosomes, compared to 10% for DMSO control. Metaphase cells imaged 30 min after RO washout or by MG132 synchronization showed no significant supernumerary centrosomes. At late stages of mitosis, 26% of the cells at telophase or undergoing cytokinesis exhibited supernumerary centrosomes compared to 11% for DMSO control. Thus, these data indicate that Piezo proteins play an important role in maintaining centrosome integrity during the different stages of mitosis but except the metaphase.

Piezo1 and 2 Can Mediate Ca^{2+} Signaling at Centrosomes. During mitosis, extremely high levels of calmodulin (CaM) activation are associated with centrosomes and mitotic spindle poles (43, 44). Although the source of Ca^{2+} ions at the centrosome is unclear, the localization of Piezo proteins at the centrosome and their ability to transmit Ca^{2+} currents prompted us to consider whether Piezo proteins contribute to Ca^{2+} signaling at the centrosome. To monitor local Ca^{2+} levels in individual C2C12 cells, we generated stable cell lines expressing the Ca^{2+}-sensitive GCaMP6 reporter targeted to different intracellular locations. GCaMP6 is a highly sensitive Ca^{2+} indicator that represents a fusion between CaM binding peptide (M13), a permuted GFP, and CaM itself (45–48). Upon Ca^{2+} binding, GCaMP6 undergoes a conformational change that increases fluorescence intensity.

One reporter line, carrying a nuclear localization signal (NLS)-tagged GCaMP6 construct, NLS-GCaMP6, showed uniform nuclear signal in interphase, but strong fluorescence at centrosomes after nuclear envelope breakdown in mitosis and subsequently around the ends of mitotic spindles (Fig. 6*A* and *SI Appendix*, Fig. S8 *A* and *B* and Movie S7). Untagged GCaMP6 reporter and the Ca^{2+} sensitive dye Fluo4-AM also showed signals at centrosomes in both interphase and mitosis (*SI Appendix*, Fig. S8 *C* and *D*), supporting the high centrosomal concentration of Ca^{2+}. The NLS-GCaMP6 line displayed most focused signals at the centrosomes and was used to monitor Ca^{2+} changes in response to Piezo modulation. As expected, 1 μM of the Ca^{2+} ionophore ionomycin and 10 μM Yoda1 both increased NLS-GCaMP6 reporter fluorescence intensity, while the calcium chelator BAPTA-AM decreased the fluorescence intensity (*SI Appendix*, Fig. S8 *A* and *B*).

We imaged Ca^{2+}-induced fluorescence intensity at centrosomes in mitotic NLS-GCaMP6 C2C12 cells 5 min after Yoda1 or GsMTx4 addition (Fig. 6*B* and *SI Appendix*, Fig. S8*E*). While Yoda1 increased the maximal fluorescence intensity at centrosomes and spindle poles by 2.2-fold compared to the level before stimulation, GsMTx4 reduced fluorescence to 60% of the level before treatment. Of note, GCaMP6 signal in the cytosol also changed proportionally, likely due to Piezo distribution in other intracellular compartments.

We further performed Piezo1 and 2 pKO in the NLS-GCaMP6 line and found that on day 1 after Piezo pKO selection, Piezo1 and 2 C2C12 pKO cells exhibited reductions in maximal fluorescence intensity at centrosomes to 44% and 34%, respectively, of the average level in Rosa26 control cells (Fig. 6*C* and *SI Appendix*, Fig. S8*F*). The difference in fluorescence was not due to changes in GCaMP6 protein levels at the centrosome, as anti-GFP IF showed similar levels of GCaMP6 protein localization at centrosomes in Rosa26 and Piezo pKO C2C12 cells (*SI Appendix*, Fig. S8*G*).

PLK1 Inhibition Abolished Yoda1-Induced Centriole Disengagement. In order to obtain a mechanistic understanding on Piezo activity modulation-induced centriole disengagement, we tested the role of Polo-like-kinase 1 (PLK1), a serin/threonine kinase that has a recognized role in coordinating procentriole maturation and centriole duplication (49–53). We found by western blots that in C2C12 cells, PLK1 expression was high in G2, low in S and M and lowest in G1 (*SI Appendix*, Fig. S9*A*). Piezo2 appeared to follow the PLK1 expression pattern by cell cycle stages while Piezo1 expression was mostly constant throughout cell cycle with a slight enrichment in G1 (*SI Appendix*, Fig. S9*A*). Of note, these experiments were performed by synchronization to G1, S, G2, and M using, respectively, 24 h serum starvation, double thymidine block, 12-h RO treatment, and plate shake-off at 30 min after RO washout.

We first tested a potent and well-studied inhibitor of PLK1, BI-2536, which was however toxic to C2C12 cells. Therefore, as an alternative, we used BI-6727, a potent and more selective PLK1 inhibitor (54). We titrated different concentrations of BI-6727 (Volasertib, 1 nM to 100 nM) in C2C12 cells, performed cell cycle analysis based on propidium iodide staining and determined the optimal working concentration in C2C12 cells as 100 nM (*SI Appendix*, Fig. S9*B*). Incubation of C2C12 cells with 100 nM BI-6727 for 18 h followed by 30-min treatment with DMSO, Yoda1 or GsTMx4 showed that BI-6727 prevented the appearance of supernumerary centrosomes shown by IF and quantification (Fig. 6 *D* and *E*). We also used IF to determine the effect of Piezo1 activation by Yoda1 on PLK1 distribution and found that PLK1 partially localized on the centrosome both before and after Yoda1 treatment (Fig. 6*F*). These data suggested that Piezo1 and 2 impact centrosomes by acting upstream of PLK1 to regulate PLK1 activity.

Discussion

The present study demonstrates that in addition to its known role in sensing forces that impinge on the cell membrane, Piezo signal transduction also operates intracellularly in the context of centrosome function and mitosis (Fig. 6*G*). We provide evidence that Piezo proteins exhibit centrosomal localization and that both Piezo hyperactivation and inhibition can induce supernumerary centrosomes and mitotic defects. This fundamental cellular function of Piezo proteins is supported by the embryonic and perinatal lethality, respectively, in *Piezo1*$^{-/-}$ and *Piezo2*$^{-/-}$ mice (8, 21). Previous studies have implicated force generation by microtubules as essential for maintaining centrosomal integrity (55), but the proteins that mediate this mechanotransduction have remained unknown. Our studies implicate Piezo proteins as key regulators of this process, which is important not only for normal cell division, but also for aberrations such as cancer which is frequently associated with supernumerary centrosomes. Perhaps the needed force balance on the microtubules explains that either hyper- or hypoactivation of Piezo proteins causes centrosomal and mitotic defects. This intriguing result is also potentially consistent with the observation of similar arthrogryposis phenotypes in humans carrying either

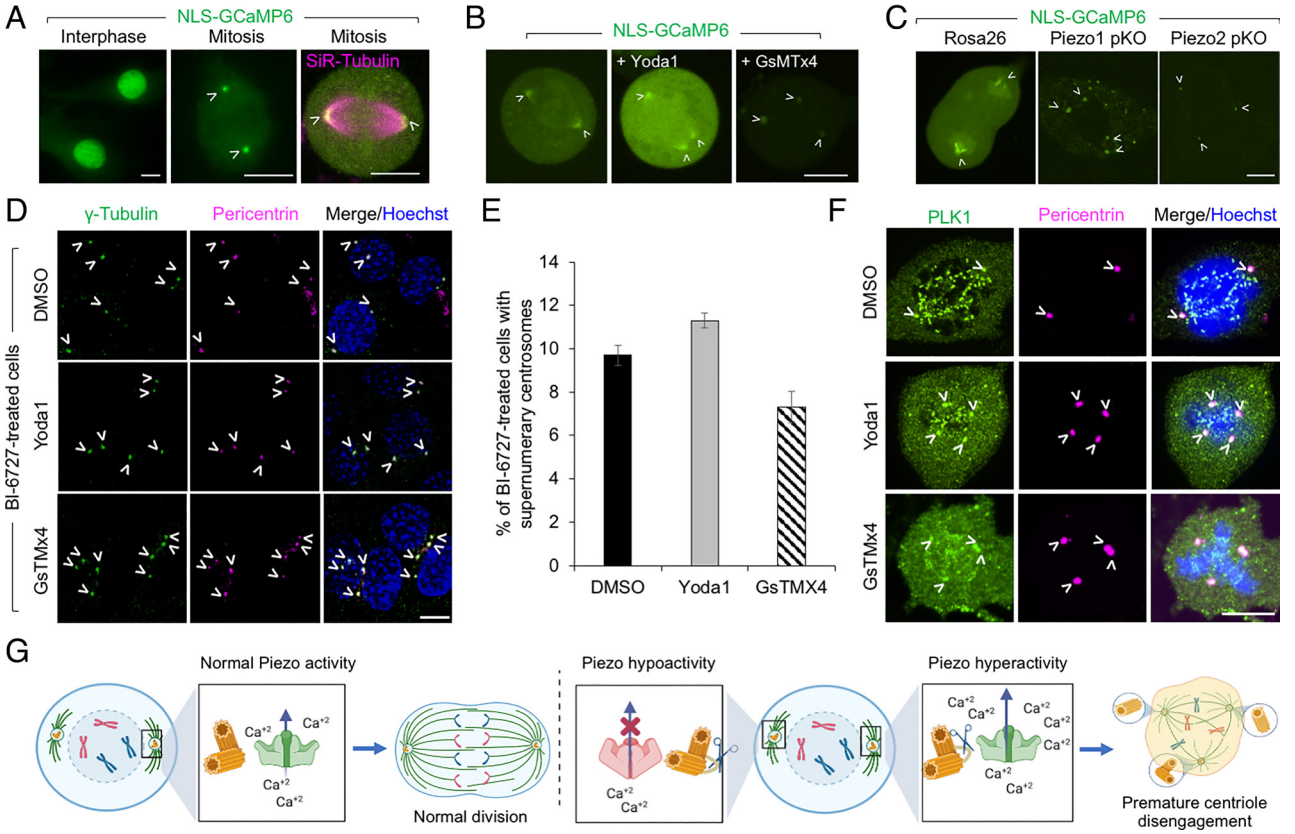

Fig. 6. Piezo modulation changes Ca^{2+} signals at the centrosome and PLK1 inhibition prevents supernumerary centrosomes. (*A*) Live images of C2C12 cells stably expressing NLS-tagged GCaMP6 Ca^{2+}-responsive fluorescence reporter construct. In interphase cells, the NLS-GCaMP6 reporter demonstrated the expected fluorescence in the nucleus (*Left*). Following nuclear envelope breakdown during early mitosis, concentrated fluorescence at the centrosomes was observed (*Middle*). In metaphase, the concentrated fluorescence was localized to the mitotic spindles, visualized also by SiR-Tubulin-staining of microtubules (magenta) (*Right*). (*B*) Live images of C2C12 cells stably expressing NLS-GCaMP6, imaged just prior to Yoda1 addition (*Left*), 5 min after Yoda1 (10 μM, *Middle*) or 5 min after GsMTx4 (5 μM, *Right*) addition. In the *Left* and *Middle* panels, the same cell was imaged before and after Yoda1 activation. (*C*) Live images of Piezo1 and 2 pKO C2C12 cells stably expressing NLS-GCaMP6 compared to an off target Rosa26 pKO control cell at day 1 post-KO selection. (*D*) IF of C2C12 cells stained with γ-Tubulin (green), Pericentrin (magenta) and DNA (blue) after treatment with the PLK1 inhibitor BI-6727 for 18 h and with Yoda1, GsTMx4 or DMSO (control) for 30 min. (*E*) Quantification of cell populations with supernumerary centrosomes for IF images in (*D*). (*F*) IF images of mitotic C2C12 cells stained for PLK1 (green), Pericentrin (magenta) and DNA (blue), fixed 30 min after addition of DMSO (control), Yoda1 or GsTMx4. No apparent changes in PLK1 localization at centrosomes were observed. (*G*) Proposed model for how Piezo-mediated Ca^{2+} signaling regulates centriole disengagement. Piezo at or near centrosomes may respond to mechanical forces transmitted by microtubules that deform presumed Piezo-containing vesicular membrane, activating Piezo to release internally stored Ca^{2+} and activating Ca^{2+}-sensitive centrosomal proteins that maintain centrosome integrity. Normal, hyperactivated, and hypoactivated Piezo states are shown. Ca^{2+} excess or deficit leads to rapid centriole disengagement. All images are maximum intensity Z projections. (Scale bars, 10 μm.) Centrosomes are marked with white arrowheads.

PIEZO2 gain- and loss-of-function mutations (15–19). However, our studies used mouse cell lines or tissues; further analyses are required to determine whether Piezo proteins play similar roles in human cells.

Our studies further suggest that premature centriole disengagement underlies the induction of supernumerary centrosomes by Piezo hyperactivation and inhibition in a PLK1-dependent manner. Interestingly, a premature centriole disengagement phenotype dependent on PLK1 activity was also observed after a prolonged RO treatment of 48 h (51). However, Piezo activity modulation-induced centriole disengagement is rapid and occurs in both synchronized and unsynchronized cells. Because PLK1 activity during early mitosis is actually required for subsequent disengagement of centrioles at late mitosis (50, 51, 56), prolonged RO treatment- and Yoda1-induced phenotypes, one slow and one fast, respectively, may be related to the same or similar downstream pathways in the "normal" centrosome cycle.

What intracellular membrane compartment Piezo proteins reside in at the centrosome is unclear. One possibility involves endosomes, which dynamically traffic and localize to the centrosome (57–60), and recent studies implicated Piezo1 in controlling endosome trafficking (25). If Piezo proteins are associated with endosomes, vesicular membrane deformation by microtubules could provide a means of transducing cytoskeletal forces to Piezo-containing membranes for Ca^{2+} release in proximity to centrosomes. Balanced cytoskeletal forces with optimal Piezo-induced local Ca^{2+} signals may act upon the pericentriolar matrix and the centrosome to regulate centriole engagement during the cell cycle (55). In this regard, many centrosomal proteins that regulate the centrosome pathway are known to be Ca^{2+}-sensitive, including Centrins, Pericentrin, Separase, and CaM (61–65). A full understanding of how Piezo mechanotransduction and Ca^{2+} signaling act at the centrosome, or intracellularly in general, will undoubtedly provide fresh insights into Piezo-mediated human diseases.

Methods

Constructs and Cell Culture. The different cell lines used in this study (Neuro-2A, C2C12, IMCD3 and HEK293T) were cultured in Dulbecco's modified Eagle's medium (DMEM) supplemented with 10% fetal bovine serum (FBS).

Mice. *Piezo2*$^{-/-}$ mice generated by breeding *Piezo2*$^{fl/fl}$ and *EIIaCre* mice (11) were purchased from The Jackson Laboratory (stock 027720).

CRISPR-Cas9 pKO. The following two Piezo sgRNAs and a control sgRNA were cloned into the lentiCRISPRv2 vector (Addgene) containing Cas9, tested in C2C12 cells and validated by western blotting.

Piezo1 exon 8 sgRNA: 5′-GTGCTTAGTGTTGAGTACCA-3′
Piezo2 exon 38 sgRNA: 5′-GGACTGCCTTGAGATCAGCA-3′
Rosa26 Off Target control sgRNA: 5′-GACTCCAGTCTTTCTAGAAGA-3′

IF. Cell lines and primary myoblasts were plated on LabTek II 4-well chamber slides, LabTek 35 mm bottom glass dishes or CELLview four-compartment dishes (Greiner Bio-One), fixed in 100% methanol for 5 min at −20 °C or 4% paraformaldehyde (PFA) for 10 min at room temperature and permeabilized with 0.1% Triton X-100 for 10 min. Cells were incubated in PBS with Tween 20 (PBST) containing 10% normal goat serum for 1 h, which minimized non-specific binding. After three washes with PBST, cells were incubated overnight at 4 °C with primary antibody.

Quantification and Statistical Analysis. Quantitative analysis for all IF experiments were performed based on n = 3 independent experiments. Statistical significance was assessed by either one-way ANOVA or two-tailed *t* test. ***, ** and * denote $P < 0.0001$, 0.001 and 0.01, respectively.

Data, Materials, and Software Availability. All study data are included in the article and/or *SI Appendix*.

ACKNOWLEDGMENTS. We thank Ardem Patapoutian for discussions, Paula Montero Llopis and Microscopy Resources on the North Quad (MicRoN) core at Harvard Medical School for microscope use and training, Maria Ericsson, Margaret Coughlin, and Anja Nordstrom from the Harvard Medical School EM Core for cell sectioning for TEM and SEM and assistance with EM imaging, Margaret Muscato, Ken Anderson, and Steve Coleman from Biovis for their assistance with iSIM imaging, Emily Cronin-Furman, Erin Powrie and Kathy Lindsley from Olympus for their assistance with STORM imaging, and Grigoriy Losyev at the flow cytometry core at Brigham and Women's Hospital for assistance with cell sorting. This work was supported by NIH grants U01 DE024443 and U01 HG007690 (R.L.M.) and by a fellowship from the Cancer Research Institute (L.D.).

Author affiliations: [a]Department of Biological Chemistry and Molecular Pharmacology, Harvard Medical School, Boston, MA 02115; [b]Program in Cellular and Molecular Medicine, Children's Hospital Boston, Boston, MA 02115; [c]Division of Genetics, Department of Medicine, Brigham and Women's Hospital, Harvard Medical School, Boston, MA 02115; [d]Biological Sciences in Dental Medicine, Harvard School of Dental Medicine, Boston, MA 02115; [e]Department of Systems Biology, Harvard Medical School, Boston, MA 02115; and [f]Renal Division, Brigham and Women's Hospital, Harvard Medical School, Boston, MA 02115

Author contributions: L.D., R.L.M., and H.W. designed research; L.D., L.M., Q.X., and Y.Z. performed research; L.D., L.M., K.A.K., and J.V.S. contributed new reagents/analytic tools; L.D., L.M., and Y.Z. analyzed data; and L.D., R.L.M., and H.W. wrote the paper.

1. B. Coste *et al.*, Piezo1 and Piezo2 are essential components of distinct mechanically activated cation channels. *Science* **330**, 55–60 (2010).
2. B. Coste *et al.*, Piezo proteins are pore-forming subunits of mechanically activated channels. *Nature* **483**, 176–181 (2012).
3. L. Volkers, Y. Mechioukhi, B. Coste, Piezo channels: From structure to function. *Pflugers. Arch.* **467**, 95–99 (2015).
4. R. Gnanasambandam, C. Bae, P. A. Gottlieb, F. Sachs, Ionic selectivity and permeation properties of human PIEZO1 channels. *PLoS One* **10**, e0125503 (2015).
5. J. Li *et al.*, Piezo1 integration of vascular architecture with physiological force. *Nature* **515**, 279–282 (2014).
6. B. Rode *et al.*, Piezo1 channels sense whole body physical activity to reset cardiovascular homeostasis and enhance performance. *Nat. Commun.* **8**, 350 (2017).
7. S. J. Allison, Hypertension: Mechanosensation by PIEZO1 in blood pressure control. *Nat. Rev. Nephrol.* **13**, 3 (2017).
8. S. S. Ranade *et al.*, Piezo1, a mechanically activated ion channel, is required for vascular development in mice. *Proc. Natl. Acad. Sci. U.S.A.* **111**, 10347–10352 (2014).
9. S. M. Cahalan *et al.*, Piezo1 links mechanical forces to red blood cell volume. *Elife* **4**, e07370 (2015).
10. A. Faucherre, J. Nargeot, M. E. Mangoni, C. Jopling, Piezo2b regulates vertebrate light touch response. *J. Neurosci.* **33**, 17089–17094 (2013).
11. S. H. Woo *et al.*, Piezo2 is required for Merkel-cell mechanotransduction. *Nature* **509**, 622–626 (2014).
12. S. S. Ranade *et al.*, Piezo2 is the major transducer of mechanical forces for touch sensation in mice. *Nature* **516**, 121–125 (2014).
13. S. H. Woo *et al.*, Piezo2 is the principal mechanotransduction channel for proprioception. *Nat. Neurosci.* **18**, 1756–1762 (2015).
14. S. L. Alper, Genetic diseases of PIEZO1 and PIEZO2 dysfunction. *Curr. Top. Membr.* **79**, 97–134 (2017).
15. B. Coste *et al.*, Gain-of-function mutations in the mechanically activated ion channel PIEZO2 cause a subtype of Distal Arthrogryposis. *Proc. Natl. Acad. Sci. U.S.A.* **110**, 4667–4672 (2013).
16. A. Delle Vedove *et al.*, Biallelic loss of proprioception-related PIEZO2 causes muscular atrophy with perinatal respiratory distress, arthrogryposis, and scoliosis. *Am. J. Hum. Genet.* **99**, 1206–1216 (2016).
17. A. T. Chesler *et al.*, The role of PIEZO2 in human mechanosensation. *N. Engl. J. Med.* **375**, 1355–1364 (2016).
18. A. A. Mahmud *et al.*, Loss of the proprioception and touch sensation channel PIEZO2 in siblings with a progressive form of contractures. *Clin. Genet.* **91**, 470–475 (2017).
19. M. J. McMillin *et al.*, Mutations in PIEZO2 cause Gordon syndrome, Marden-Walker syndrome, and distal arthrogryposis type 5. *Am. J. Hum. Genet.* **94**, 734–744 (2014).
20. M. I. Rauchman, S. K. Nigam, E. Delpire, S. R. Gullans, An osmotically tolerant inner medullary collecting duct cell line from an SV40 transgenic mouse. *Am. J. Physiol.* **265**, F416–F424 (1993).
21. K. Nonomura *et al.*, Piezo2 senses airway stretch and mediates lung inflation-induced apnoea. *Nature* **541**, 176–181 (2017).
22. S. A. Gudipaty *et al.*, Mechanical stretch triggers rapid epithelial cell division through Piezo1. *Nature* **543**, 118–121 (2017).
23. B. J. McHugh *et al.*, Integrin activation by Fam38A uses a novel mechanism of R-Ras targeting to the endoplasmic reticulum. *J. Cell Sci.* **123**, 51–61 (2010).
24. T. Zhang, S. Chi, F. Jiang, Q. Zhao, B. Xiao, A protein interaction mechanism for suppressing the mechanosensitive Piezo channels. *Nat. Commun.* **8**, 1797 (2017).
25. J. Carrillo-Garcia *et al.*, The mechanosensitive Piezo1 channel controls endosome trafficking for an efficient cytokinetic abscission. *Sci. Adv.* **7**, eabi7785 (2021).
26. M. Kwon *et al.*, Mechanisms to suppress multipolar divisions in cancer cells with extra centrosomes. *Genes. Dev.* **22**, 2189–2203 (2008).
27. E. A. Nigg, A. J. Holland, Once and only once: Mechanisms of centriole duplication and their deregulation in disease. *Nat. Rev. Mol. Cell Biol.* **19**, 297–312 (2018).
28. L. T. Vassilev *et al.*, Selective small-molecule inhibitor reveals critical mitotic functions of human CDK1. *Proc. Natl. Acad. Sci. U.S.A.* **103**, 10660–10665 (2006).
29. T. A. Rando, H. M. Blau, Primary mouse myoblast purification, characterization, and transplantation for cell-mediated gene therapy. *J. Cell. Biol.* **125**, 1275–1287 (1994).
30. R. Syeda *et al.*, Chemical activation of the mechanotransduction channel Piezo1. *Elife* **4**, e07369 (2015).
31. J. J. Lacroix, W. M. Botello-Smith, Y. Luo, Probing the gating mechanism of the mechanosensitive channel Piezo1 with the small molecule Yoda1. *Nat. Commun.* **9**, 2029 (2018).
32. E. L. Evans *et al.*, Yoda1 analogue (Dooku1) which antagonizes Yoda1-evoked activation of Piezo1 and aortic relaxation. *Br. J. Pharmacol.* **175**, 1744–1759 (2018).
33. K. Nonomura *et al.*, Mechanically activated ion channel PIEZO1 is required for lymphatic valve formation. *Proc. Natl. Acad. Sci. U.S.A.* **115**, 12817–12822 (2018).
34. Y. Wang *et al.*, A lever-like transduction pathway for long-distance chemical- and mechano-gating of the mechanosensitive Piezo1 channel. *Nat. Commun.* **9**, 1300 (2018).
35. C. Bae, F. Sachs, P. A. Gottlieb, The mechanosensitive ion channel Piezo1 is inhibited by the peptide GsMTx4. *Biochemistry* **50**, 6295–6300 (2011).
36. C. Alcaino, K. Knutson, P. A. Gottlieb, G. Farrugia, A. Beyder, Mechanosensitive ion channel Piezo2 is inhibited by D-GsMTx4. *Channels (Austin)* **11**, 245–253 (2017).
37. R. Gnanasambandam *et al.*, GsMTx4: Mechanism of inhibiting mechanosensitive ion channels. *Biophys. J.* **112**, 31–45 (2017).
38. W. Lee *et al.*, Synergy between Piezo1 and Piezo2 channels confers high-strain mechanosensitivity to articular cartilage. *Proc. Natl. Acad. Sci. U.S.A.* **111**, E5114–E5122 (2014).
39. S. A. Godinho, D. Pellman, Causes and consequences of centrosome abnormalities in cancer. *Philos. Trans. R. Soc. Lond. B. Biol. Sci.* **369**, 20130467 (2014).
40. M. Karki, N. Keyhaninejad, C. B. Shuster, Precocious centriole disengagement and centrosome fragmentation induced by mitotic delay. *Nat. Commun.* **8**, 15803 (2017).
41. T. Wilhelm *et al.*, Mild replication stress causes chromosome mis-segregation via premature centriole disengagement. *Nat. Commun.* **10**, 3585 (2019).
42. F. Alisch *et al.*, Familial Gordon syndrome associated with a PIEZO2 mutation. *Am. J. Med. Genet. A* **173**, 254–259 (2017).
43. K. Torok, M. Wilding, L. Groigno, R. Patel, M. Whitaker, Imaging the spatial dynamics of calmodulin activation during mitosis. *Curr. Biol.* **8**, 692–699 (1998).
44. R. K. Mallampalli, J. R. Glasser, T. A. Coon, B. B. Chen, Calmodulin protects Aurora B on the midbody to regulate the fidelity of cytokinesis. *Cell Cycle* **12**, 663–673 (2013).
45. T. W. Chen *et al.*, Ultrasensitive fluorescent proteins for imaging neuronal activity. *Nature* **499**, 295–300 (2013).
46. R. Cohen, D. A. Holowka, B. A. Baird, Real-time imaging of Ca(2+) mobilization and degranulation in mast cells. *Methods Mol. Biol.* **1220**, 347–363 (2015).
47. T. X. Dong *et al.*, T-cell calcium dynamics visualized in a ratiometric tdTomato-GCaMP6f transgenic reporter mouse. *Elife* **6** (2017).
48. J. Nakai, M. Ohkura, K. Imoto, A high signal-to-noise Ca(2+) probe composed of a single green fluorescent protein. *Nat. Biotechnol.* **19**, 137–141 (2001).
49. B. R. Mardin, E. Schiebel, Breaking the ties that bind: New advances in centrosome biology. *J. Cell Biol.* **197**, 11–18 (2012).
50. A. Shukla, D. Kong, M. Sharma, V. Magidson, J. Loncarek, Plk1 relieves centriole block to reduplication by promoting daughter centriole maturation. *Nat. Commun.* **6**, 8077 (2015).
51. J. Loncarek, P. Hergert, A. Khodjakov, Centriole reduplication during prolonged interphase requires procentriole maturation governed by Plk1. *Curr. Biol.* **20**, 1277–1282 (2010).
52. W. J. Wang, R. K. Soni, K. Uryu, M. F. Tsou, The conversion of centrioles to centrosomes: Essential coupling of duplication with segregation. *J. Cell Biol.* **193**, 727–739 (2011).
53. R. K. Soni, M. F. Tsou, A cell-free system for real-time analyses of centriole disengagement and centriole-to-centrosome conversion. *Methods Mol. Biol.* **1413**, 197–206 (2016).
54. P. Lenart *et al.*, The small-molecule inhibitor BI 2536 reveals novel insights into mitotic roles of polo-like kinase 1. *Curr. Biol.* **17**, 304–315 (2007).
55. G. Cabral, S. S. Sans, C. R. Cowan, A. Dammermann, Multiple mechanisms contribute to centriole separation in C. elegans. *Curr. Biol.* **23**, 1380–1387 (2013).

56. M. F. Tsou *et al.*, Polo kinase and separase regulate the mitotic licensing of centriole duplication in human cells. *Dev. Cell* **17**, 344–354 (2009).
57. H. Hehnly, C. T. Chen, C. M. Powers, H. L. Liu, S. Doxsey, The centrosome regulates the Rab11-dependent recycling endosome pathway at appendages of the mother centriole. *Curr. Biol.* **22**, 1944–1950 (2012).
58. H. F. Hung, H. Hehnly, S. Doxsey, Methods to analyze novel liaisons between endosomes and centrosomes. *Methods Cell Biol.* **130**, 47–58 (2015).
59. A. Vertii, H. Hehnly, S. Doxsey, The centrosome, a multitalented renaissance organelle. *Cold Spring Harb. Perspect. Biol.* **8**, a025049 (2016).
60. J. Saraste, M. Marie, Intermediate compartment (IC): From pre-Golgi vacuoles to a semi-autonomous membrane system. *Histochem. Cell Biol.* **150**, 407–430 (2018), 10.1007/s00418-018-1717-2.
61. R. Agarwal, O. Cohen-Fix, Mitotic regulation: The fine tuning of separase activity. *Cell Cycle* **1**, 255–257 (2002).
62. B. J. Galletta *et al.*, Drosophila pericentrin requires interaction with calmodulin for its function at centrosomes and neuronal basal bodies but not at sperm basal bodies. *Mol. Biol. Cell* **25**, 2682–2694 (2014).
63. C. H. Yang, C. Kasbek, S. Majumder, A. M. Yusof, H. A. Fisk, Mps1 phosphorylation sites regulate the function of centrin 2 in centriole assembly. *Mol. Biol. Cell* **21**, 4361–4372 (2010).
64. D. B. Sawant *et al.*, Centrin 3 is an inhibitor of centrosomal Mps1 and antagonizes centrin 2 function. *Mol. Biol. Cell* **26**, 3741–3753 (2015).
65. L. Schockel, M. Mockel, B. Mayer, D. Boos, O. Stemmann, Cleavage of cohesin rings coordinates the separation of centrioles and chromatids. *Nat. Cell Biol.* **13**, 966–972 (2011).